Journal of Radioanalytical and Nuclear Chemistry (2019) 322:319–330
https://doi.org/10.1007/s10967-019-06739-8

^{210}Pb and ^{137}Cs based techniques for the estimation of sediment chronologies and sediment rates in the Anzali Lagoon, Caspian Sea

A. Abbasi[1]

Received: 5 April 2019 / Published online: 4 September 2019

Abstract
^{137}Cs and ^{210}Pb based sediment chronology methods, along with an HPGe gamma-ray spectrometry system, were applied to estimating of sediment accumulative rates (SAR), sedimentation rate (SR) and sedimentation chronology in the Anzali Lagoon. Sedimentation chronology was calculated according to the $^{210}Pb_{ex}$ based-models including; the constant rate of supply, constant initial concentration and ^{137}Cs peak-technique. The SAR value were ranged from 0.12 g cm^{-2} year^{-1} in core-2 to 0.21 g cm^{-2} year^{-1} in core-3. The results showed that the average of SR and SAR values after 1986; interval were 22% and 54% more than between 1963 and 1986 intervals.

Keywords ^{137}Cs · ^{210}Pb · Dating method · Sediment rates (SR) · Sediment accumulative rate (SAR)

Introduction

Sediment history in the lagoons and large lakes can provide information about environmental changes, and shows chronological records in sediment layers [1–3]. The varve chronologies-based methods are applied to determine sediment chronology. For younger sediment than 100–120 years, Lead-210 (^{210}Pb, $T_{1/2}=22.3$ years) dating method is common. This method include the constant rate of supply (CRS) model and constant initial concentration (CIC) model [4]. Another dating method is ^{137}Cs based method that derived from nuclear fallout studies [5].

The man-made radioisotope of ^{137}Cs ($T_{1/2}$ = 30.17 years) produced in nuclear fission reactions has entered into the atmosphere in irregularly varying amounts since 1945 [6, 7]. Nuclear accidents such as the Chernobyl accident and atmospheric nuclear weapons testing of the 1950s released large amounts of fission product like ^{137}Cs into the environment [8].

Considering the ^{137}Cs half-life, makes it's as measurable tracer in the early 1950s, so sediment profile in a core along with ^{137}Cs detectable activity has chronology application [9, 10]. In practical studies, ^{137}Cs distributions in sediments profile derived from atmospheric nuclear weapons testing in the 1960s and the Chernobyl accident in 1986 were used as time markers to calculate sediment accumulation rates in lakes and reservoirs [11–14]. Determination of the sedimentation rates with the ^{137}Cs and ^{210}Pb method is suitable for sediments of up to 100 -120 years old [15–17].

Today it is accepted that two major challenge of global warming and land use change have caused significant changes of sediment distribution rates within the different parts of the fluvial system during recent decades. Schumm [18] divided a fluvial system into three zones: an upland erosion zone, a transportation zone and a sedimentation zone. Climate changing and/or human activities may result in changes in erosion and transportation processes in the first two zones, and these will influence the sedimentation rate in the third zone [19].

In this research, due to recent concerns about unusual changes of the Anzali Lagoon ecosystem, with emphasizes the effects of short-term natural changes in the coastal lagoons about anthropogenic effects, and demonstrates that rapid change is not only due to human action but also due to rapid sea-level change (Fig. 1). The hypothesis of this research was an investigation of sediment age of the Anzali Lagoon to determine entering and displaced sediment rate in Lagoon. By understanding the annual sedimentation rate, this can provide suitable planning for the lagoon conservation and sediment management. For this reason, we apply the sedimentary analyses method in the Anzali Lagoon. For

✉ A. Abbasi
akbar.abbasi@emu.edu.tr; akbar.abbasi@kyrenia.edu.tr

1 Faculty of Engineering, University of Kyrenia, TRNC, Via Mersin 10, Turkey

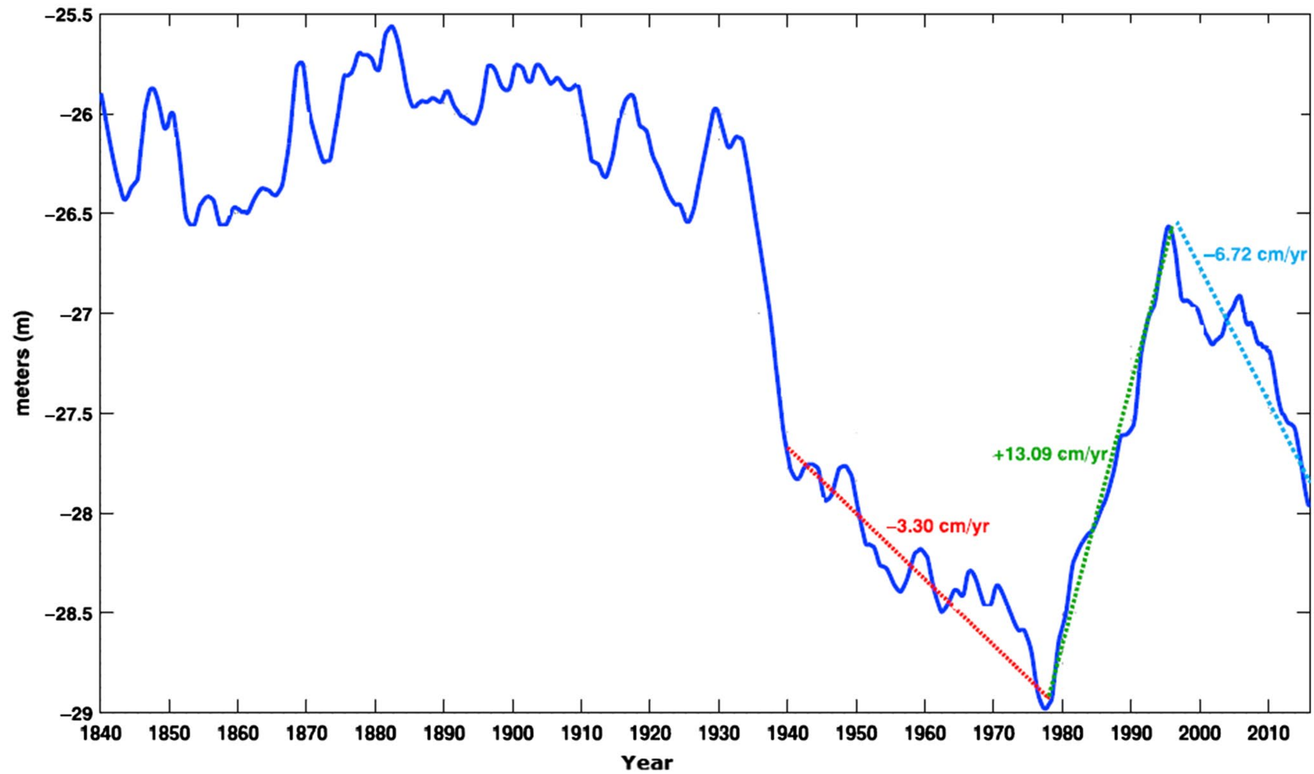

Fig. 1 The average monthly mean Caspian Sea level (CSL) changes (1840–2015), [22]

this purpose, the distribution of the ^{137}Cs and ^{210}Pb in sediment core profiles were measured. The sediment accumulative rates (SAR), sediment chronology and sedimentation rates (SR) after the 1960s were carried out by means of ^{137}Cs and ^{210}Pb based dating methods. Whereas, spatially concentrated on SR and SARs in the last decades. Also, the other purpose was the study of SR and SARs in 1963–1986 and after 1986 periods.

Materials and methods

Study area description

The study area was selected the Anzali Lagoon with a wet weather marsh ecosystem where this lagoon is one of 10 well-known lagoons in the world located in the western south of Caspian Sea, between 49.25 to 49.5 E and 37.25 to 37.5 N. (Figure 2). The area of the Anzali Lagoon complex covers 150 km^2 [20] and the distance from Chernobyl nuclear power plant approximately is 2000 km.

The average lagoon level is about − 26.2 m. Also, water depth range is between 1 and 3.5 m. Lagoon has a Mediterranean climate with abundant precipitation of 1600 mm (in mean annual precipitation). More than fifteen perennial and ephemeral rivers originating from the Alborz and Talesh Mountains discharge into the lagoon. The geology of the Lagoon basin is characterized by rocks of the Devonian-Carboniferous Gneiss, Precambrian Metamorphic Complex (schist), migmatite and mica schist rocks. These rocks are overlain by middle Triassic basic to ultrabasic rocks. Green micaceous schists and sandstones of Jurassic age, limestone of Cretaceous age, and green and red marls of Pliocene age also form outcrops in the area. The sediment origin of the Lagoon is from three sources: (a) sediments deposited from rivers; (b) erosion of Alborz mountain (coarse sediments); and (c) marine deposition (includes shelly sands) [21].

Various plants such as Phragmites, Aquatic macrophytes and Azolla as well as special morphology with some transferring channels to the Caspian Sea make the lagoon a touristic destination. Different uses of the Lagoon by residents such as the application of its water for agriculture, the lagoon plant as forage for domestic animals, its suitable place for birds and fishing makes it essential for monitoring of ^{137}Cs activity concentration in sediment profiles.

Field sampling

A total of four sediment cores were collected from different locations of the Anzali Lagoon, via a vibra-coring unit with portable by boat in September 2014. The core (inside diameter of φ = 12 cm) length was variable from 45 to 57 cm and water

Fig. 2 Geographical location of the Anzali Lagoon ecosystem and sampling points

depth was from 1.5 to 6 m. The core tubes were transferred vertically to the laboratory where they sliced at 1 cm thick layers.

Sediment analysis

Each sediment sample weighed and dried at ~ 80 °C for 12 h to measuring before and after drying in order to determine the dry weight of the sample. The porosity of samples was calculated using the following equation [23]:

$$\phi = \frac{f_w}{\left[f_w + \left(1 - f_w\right).\left(\rho_w/\rho_s\right)\right]} \quad (1)$$

where ϕ is the porosity, f_w is the fraction of water in the fresh sediments $(1 - \frac{dry\ wt}{fres\ wt})$, ρ_w is the density of pure water (~ 1 g cm^{-3}), and ρ_s is the density of the dry solids (~ 2.5 g cm^{-3}).

Deeper sediments were a combination of fine and medium grains such as silty, fine and sand. While the surface sediments content was a mixture of silts, clays and mud.

To take into account sediment compaction dating must be performed as a function of mass depth m (kg m^{-2}). For this porpose the mass depth (m_i) of layer (i) (kg m^{-2}), was calculated by:

$$m_i = \sum_{j=1}^{j=i} \frac{\Delta m_j}{s}$$

where Δm_j is the dry mass of section i (kg), experimentally determined and S is core cross-section (m^2).

Gamma spectrometry analysis

The gamma-ray spectra system used to measure of the prepared samples. This system consists of a typical high-resolution gamma spectrometer (SILENA) based on a coaxial P-type HPGe detector with cylindrical shielding, a relative photopeak efficiency of 80% and an energy resolution of 1.80 keV FWHM for the 1332 keV gamma-ray line of ^{60}Co. Before the sample measurements, the environmental gamma background (B.G) in the laboratory site was determined using an empty 100 ml cylindrical beaker under identical measurement conditions. Each sample was transferred to 100 ml sealed polyethylene cylindrical beaker and stored to receiving equilibrium between parent (^{226}Ra) and daughters (^{214}Pb, ^{214}Bi) radionuclides. After then the sample put into the shielded HPGe detector and measured for an accumulated period of 86,000s [24]. Commercial software Gamma 2000 was used for data analysis [25]. The ^{137}Cs, ^{226}Ra and ^{210}Pb activity concentrations were determined for each of the measured samples together with their corresponding total uncertainties. Activities concentration of ^{137}Cs was calculated due to 661.6 keV photopeak energy line. The ^{210}Pb activity concentration was measured with 46.5 keV gamma line energy. Also, the ^{226}Ra was measured using its decay product gamma emitters of ^{214}Pb (295 keV, 351 keV), ^{214}Bi (609 keV). The detector efficiency calibration was performed by using the IAEA-385, IAEA-375, and IAEA-384 for quality assurance reference materials produced by IAEA. The radionuclides concentration was presented in the datasheet with a 95% confidence level and all the radionuclides concentration corrected to the using date.

Activity concentration of radionuclides (A) in Bq kg^{-1} can be calculated by [26]:

$$A = \frac{N - B}{t \times p_\gamma \times ef \times m} \tag{2}$$

where N is the count rate of the sample, B is the background, t is the counting time (s), P_γ is the probability of gamma decay (%), ef—detector efficiency (%), m is the mass (kg) of the soil or sediment sample.

The minimum detectable activity (MDA) was calculated using the following equation:

$$MDA = \frac{LLD}{t \times p_\gamma \times ef \times m} \tag{3}$$

The lower limit of detection (LLD), was calculated by using the relation $LLD = 4.66\sqrt{F_c}$ where F_c is the Compton background in the region of the selected gamma-ray spectrum with a 96% confidence [27].

Uncertainty calculation

Uncertainty assessment is necessary to each calculation, the activity concentration uncertainty (U_A) calculated by the following equation:

$$\frac{U_A}{A} = \sqrt{\left(\frac{U_N}{N}\right)^2 + \left(\frac{U_B}{B}\right)^2 + \left(\frac{U_\varepsilon}{\varepsilon}\right)^2 + \left(\frac{U_M}{M}\right)^2 + \left(\frac{U_{P_\gamma}}{P_\gamma}\right)^2} \tag{4}$$

where U_N is sample counting uncertainty; U_B, background counting uncertainty; U_ε, efficiency uncertainty, U_M, mass measurements uncertainty and U_{P_γ}, gamma line energy uncertainty (for example this uncertainty for ^{137}Cs is 0.24% of intensity) [28].

Sediment chronologic models

According to some reports, it is possible to use the ^{137}Cs depth profile within such sediment deposits to identify the first peaks of ^{137}Cs activity corresponding to the year of maximum nuclear weapons testing fallout (1963) and the second peaks of ^{137}Cs activity related to the occurrence of the Chernobyl accident 1986 [29–34].

The other models that are used to estimate the chronology in this study are the constant initial concentration (CIC) model by unsupported $^{210}Pb_{ex}$ (excess ^{210}Pb or ^{210}Pb–^{226}Ra) [35] and the constant rate of supply (CRS) model with unsupported $^{210}Pb_{ex}$ [36].

^{137}Cs chronology

It is evident that the magnitude of ^{137}Cs activity has two peaks in all core sampling points. This procedure provides the possibility of calculating sedimentation rates during the periods 1963–1986 and 1986 to the present. However, in order to interpret the ^{137}Cs concentration in sediment profiles need to consider the various factors on the profiles. So, in this method, the evaluation result of sedimentation rates is average on interval times.

Where the 1963 peak could be observed in the ^{137}Cs vertical sediment profile, the average sedimentation rate (SR) R_t (cm year^{-1}) for the period of 1963–1986 was calculated as follows equation [37]:

$$R_t = \frac{D(t)_{1963} - D(t)_{1986}}{T_{1963-1986}} \tag{5}$$

where $D(t)_{1963}$ is the depth of the 1963 ^{137}Cs peak, (cm); $D(t)_{1986}$ is the depth of the 1986 ^{137}Cs peak, (cm) and $T_{1963-1986}$ is the interval time from 1963 to 1986.

^{210}Pb chronology

The constant rate of supply (CRS) model was used to unsupported ^{210}Pb ($^{210}Pb_{ex}$) inventories evaluated by subtraction of ^{210}Pb supported by ^{226}Ra to generate ages. Whereas, the total ^{210}Pb concentration in sediments including two sections, unsupported which deposited from the atmosphere and supported ^{210}Pb activity that produces inside the matrix of parent radionuclide ^{226}Ra. The CRS model in each of the cores was calculated from the following equation [38]:

$$\sum I_m = \left(\sum I_\infty\right)(1 - e^{-\lambda_{Pb} t}) \quad (6)$$

where $\sum I_m$ is the $^{210}Pb_{ex}$ concentration in mass depth (Bq cm^{-2}), $\sum I_\infty$ is the total concentration of $^{210}Pb_{ex}$ in sediment column (Bq cm^{-2}), and λ_{Pb} is decay constant of ^{210}Pb (0.03118 year^{-1}). The age of the sediment layer t_{CRS} is expressed by:

$$t_{CRS} = -\frac{\ln\left(1 - \frac{\sum I_m}{\sum I_\infty}\right)}{\lambda_{Pb}} \quad (7)$$

The CIC model was applied to calculate sediment layer ages in core samples. According to CIC model, the specific activity in the surface deposits will always be constant because due to sediment flux changes, sweeping of ^{210}Pb from the water column will also change [39–41]. According to the CIC model, the age of the sediment layer t_{CIC} is described as follows:

$$t_{CIC} = -\frac{\ln\left(\frac{A_M}{A_0}\right)}{\lambda_{Pb}} \quad (8)$$

where A_M is the $^{210}Pb_{ex}$ activity concentration in cumulative mass depth "M" (Bq g^{-1}), A_0 is the $^{210}Pb_{ex}$ activity concentration in the water–sediment interface (Bq g^{-1}) and λ_{Pb} is decay constant of ^{210}Pb.

This model was applied only for comparing the results with the CRS model. The main assumption of this model is that the proportion between ^{210}Pb flux to the sediments and the accumulative mass rates is constant along with the entire core. Whereas the accumulative mass rates will be changed throughout of core, so the results of this model are without good precisions, and we ignore the results of that report.

Results

According to our investigation, there is no study on the radioactivity concentration of ^{137}Cs and ^{210}Pb in the Anzali Lagoon sediments profiles, when this project has done (2018). In the present study, we measured the concentration of ^{137}Cs and ^{210}Pb in the Anzali Lagoon sediments from 0 to 50 cm with dividing into 1 cm intervals. The water depth and other characteristics of sediment sampling points are shown in Table 1. The water depth in four core collections ranged from 1.2 m (Core-4) to 5.8 m (Core-3). The porosity value range and average of core-1, core-2, core-3 and core-4 were 0.72 ± 0.01–0.81 ± 0.02 (0.78 ± 0.02), 0.70 ± 0.01–0.84 ± 0.04 (0.82 ± 0.03), 0.75 ± 0.02–0.85 ± 00.5 (0.79 ± 0.04) and 0.71 ± 0.02–0.88 ± 0.04 (0.84 ± 0.03), respectively are summarized in Table 1.

The activity concentration of ^{137}Cs in selected sediment profiles in depth with an interval of 1 cm was measured (Table 2). The minimum and maximum activity concentration range in Core-1 was 2.51 ± 0.02 - 65.28 ± 4.38 Bq kg^{-1} corresponding to depth 42 and 24 cm, respectively. This conformity for core-2, core-3, and core-4 were 3.62 ± 0.05 Bq kg^{-1} (48 cm)—62.15 ± 5.31 Bq kg^{-1} (22 cm), 3.19 ± 0.02 Bq kg^{-1} (44 cm)—61.76 ± 4.28 Bq kg^{-1} (23) and 3.03 ± 0.02 Bq kg^{-1} (46 cm)—73.50 ± 5.27 Bq kg^{-1} (25 cm), respectively. The median of activity concentration range was 24.95 ± 2.06 Bq kg^{-1}(core-4) to 32.65 ± 3.01 Bq kg^{-1} (core-2). ^{137}Cs activity concentration profiles from the four sampling locations are presented in Fig. 3.

The total activity concentration of $^{210}Pb_{ex}$ were ranged from 11.26 ± 0.07 Bq kg^{-1} to 218.42 ± 12.51 Bq kg^{-1} and ^{226}Ra activity concentration was ranged from 3.18 ± 0.16 Bq kg^{-1} to 34.52 ± 2.77 Bq kg^{-1} in the Core -1 samples, from 9.40 ± 0.24 Bq kg^{-1} to 230.42 ± 11.38 Bq kg^{-1} and ^{226}Ra activity concentration was ranged from < MDA (MDA_{226Ra} = 1.2 Bq kg^{-1}) to 28.15 ± 1.27 Bq kg^{-1}

Table 1 The characteristics of core sampling points

Sample code	Sampling location coordinates		Core length[a] (cm)	Water depth[a] (m)	Max–min (average)[a] porosity
	Latitude (N)	Longitude (E)			
Core-1	37, 26, 24.449	49, 24, 22.155	50 ± 3	2.8 ± 0.2	0.72 ± 0.01–0.81 ± 0.02 (0.78 ± 0.02)
Core-2	37, 27, 39.168	49, 21, 02.228	49 ± 2	3.4 ± 0.3	0.70 ± 0.01–0.84 ± 0.04 (0.82 ± 0.03)
Core-3	37, 30, 04.647	49, 17, 56.893	45 ± 1	5.8 ± 0.6	0.75 ± 0.02–0.85 ± 00.5 (0.79 ± 0.04)
Core-4	37, 29, 28.581	49, 20, 35.820	49 ± 2	1.2 ± 0.1	0.71 ± 0.02–0.88 ± 0.04 (0.84 ± 0.03)

[a]Uncertainties are considered within one standard deviation

Table 2 ^{137}Cs and ^{210}Pb$_{ex}$ activity concentration in sediment profiles of four core sampling locations

Depth (cm)	Activity concentration (Bq kg^{-1})							
	Core-1		Core-2		Core-3		Core-4	
	^{137}Cs	^{210}Pb$_{ex}$	^{137}Cs	^{210}Pb$_{ex}$	^{137}Cs	^{210}Pb$_{ex}$	^{137}Cs	^{210}Pb$_{ex}$
1	15.27 ± 1.03	218.42 ± 12.51	12.49 ± 0.81	230.42 ± 11.38	10.38 ± 0.52	184.52 ± 12.57	18.42 ± 0.48	305.22 ± 14.08
2	19.34 ± 0.14	191.27 ± 8.14	10.21 ± 0.47	226.01 ± 14.06	11.92 ± 0.24	191.28 ± 15.36	9.74 ± 0.51	297.05 ± 12.54
3	18.50 ± 0.13	184.02 ± 9.28	16.17 ± 0.18	213.30 ± 12.35	9.05 ± 0.18	190.13 ± 12.80	11.3 ± 0.20	263.47 ± 14.30
4	21.25 ± 0.28	180.14 ± 11.62	15.02 ± 0.35	186.51 ± 10.51	15.98 ± 0.14	172.19 ± 12.00	19.87 ± 0.71	222.73 ± 9.38
5	19.98 ± 0.91	173.22 ± 10.88	18.94 ± 0.28	198.60 ± 10.42	15.24 ± 0.53	164.08 ± 10.49	15.91 ± 0.64	205.56 ± 7.31
6	26.32 ± 1.04	160.51 ± 3.45	27.30 ± 0.57	176.37 ± 7.81	22.38 ± 0.48	160.71 ± 9.25	20.97 ± 1.02	186.19 ± 8.65
7	25.08 ± 1.30	159.47 ± 6.04	28.68 ± 1.24	188.54 ± 8.15	25.30 ± 0.35	167.39 ± 10.87	12.6 ± 0.30	173.88 ± 7.42
8	29.17 ± 1.05	153.00 ± 7.52	33.70 ± 2.11	150.14 ± 13.45	28.62 ± 0.99	153.84 ± 10.53	18.03 ± 0.85	176.42 ± 9.15
9	30.05 ± 1.25	149.50 ± 10.53	31.04 ± 2.51	156.08 ± 11.07	34.03 ± 1.24	147.52 ± 9.36	24.39 ± 0.97	154.91 ± 11.35
10	34.62 ± 0.97	151.39 ± 4.08	32.65 ± 1.68	152.62 ± 7.21	32.07 ± 2.40	144.94 ± 10.85	28.6 ± 1.50	155.03 ± 10.02
11	31.07 ± 1.32	142.27 ± 7.39	35.89 ± 4.05	148.05 ± 6.94	36.41 ± 5.01	132.73 ± 7.07	35.01 ± 0.68	141.57 ± 7.28
12	36.15 ± 1.07	148.33 ± 8.22	32.16 ± 2.34	140.25 ± 7.02	42.35 ± 3.81	126.45 ± 8.68	32.6 ± 2.04	132.42 ± 11.58
13	39.02 ± 2.46	145.26 ± 6.18	38.68 ± 2.51	138.64 ± 5.85	40.25 ± 6.02	122.30 ± 7.09	44.05 ± 3.15	137.95 ± 12.00
14	38.04 ± 1.65	140.90 ± 5.25	41.17 ± 4.02	156.32 ± 8.19	29.39 ± 2.54	116.46 ± 6.15	35.08 ± 2.45	126.46 ± 8.09
15	41.65 ± 0.58	136.82 ± 4.13	40.25 ± 3.73	127.91 ± 4.23	38.04 ± 3.69	104.87 ± 5.03	39.42 ± 4.81	129.57 ± 10.22
16	47.36 ± 2.32	142.68 ± 5.97	40.58 ± 2.38	110.74 ± 7.01	42.17 ± 4.07	95.70 ± 4.18	38.55 ± 2.59	126.40 ± 8.32
17	45.30 ± 1.05	127.31 ± 5.23	46.41 ± 4.57	116.28 ± 5.48	48.86 ± 3.91	93.64 ± 2.41	46.28 ± 5.21	117.06 ± 7.35
18	51.06 ± 0.99	138.02 ± 4.61	48.36 ± 3.64	123.01 ± 3.52	45.03 ± 4.08	97.32 ± 2.35	48.31 ± 4.87	119.47 ± 4.22
19	49.45 ± 1.82	132.41 ± 5.03	52.81 ± 4.80	104.39 ± 6.84	42.37 ± 5.67	88.06 ± 3.47	45.11 ± 5.20	104.35 ± 4.65
20	58.64 ± 5.34	120.70 ± .3.45	51.35 ± 5.29	110.53 ± 5.22	55.00 ± 8.20	80.31 ± 2.35	52.03 ± 2.85	100.87 ± 3.05
21	56.31 ± 3.71	122.84 ± 5.09	56.74 ± 5.37	95.42 ± 4.95	46.38 ± 5.31	74.95 ± 1.88	49.39 ± 3.71	81.13 ± 3.44
22	60.03 ± 5.64	117.50 ± 4.01	62.15 ± 4.09	98.02 ± 5.05	59.02 ± 4.97	72.64 ± 3.07	55.08 ± 3.26	85.16 ± 2.01
23	63.08 ± 7.00	91.64 ± 6.18	58.91 ± 3.22	106.51 ± 7.00	61.76 ± 5.60	70.13 ± 1.68	59.71 ± 3.81	72.90 ± 2.00
24	65.28 ± 4.39	107.43 ± 9.05	57.10 ± 7.03	86.34 ± 4.83	56.02 ± 5.04	70.09 ± 1.06	68.94 ± 5.07	70.28 ± 1.58
25	64.97 ± 4.15	88.03 ± 6.55	52.38 ± 2.61	86.28 ± 7.06	52.86 ± 4.21	63.05 ± 1.99	73.50 ± 5.36	69.94 ± 1.07
26	62.41 ± 6.47	82.46 ± 5.17	55.21 ± 5.75	74.06 ± 2.50	55.00 ± 3.51	66.29 ± 2.82	59.45 ± 4.21	66.00 ± 2.04
27	58.52 ± 3.51	59.72 ± 3.61	48.05 ± 3.24	79.21 ± 4.07	48.91 ± 5.05	58.47 ± 1.40	55.69 ± 3.02	61.34 ± 1.65
28	54.00 ± 2.60	74.05 ± 3.54	49.19 ± 2.61	70.08 ± 2.44	40.17 ± 3.68	52.34 ± 1.64	47.01 ± 2.68	57.85 ± 1.05
29	53.04 ± 4.08	51.95 ± 2.17	46.92 ± 3.50	75.14 ± 3.61	37.08 ± 2.01	55.01 ± 1.59	46.58 ± 3.51	60.57 ± 2.12
30	49.80 ± 4.55	55.27 ± 1.80	42.35 ± 4.08	68.97 ± 2.47	30.02 ± 2.84	46.21 ± 1.38	38.92 ± 3.41	51.06 ± 0.94
31	46.71 ± 2.46	56.08 ± 2.19	38.64 ± 3.62	69.05 ± 3.99	26.07 ± 2.20	37.14 ± 1.24	47.03 ± 5.02	45.00 ± 0.44
32	42.05 ± 5.07	50.28 ± 1.68	39.31 ± 2.00	65.07 ± 2.15	28.19 ± 1.09	35.85 ± 0.99	32.61 ± 3.22	47.09 ± 0.62
33	36.31 ± 3.19	43.07 ± 2.01	42.08 ± 3.91	34.19 ± 2.06	28.77 ± 1.57	33.05 ± 1.05	24.95 ± 1.07	42.71 ± 0.97
34	29.00 ± 2.71	26.71 ± 0.84	36.17 ± 2.58	31.82 ± 1.95	22.51 ± 1.03	30.12 ± 1.41	25.01 ± 2.01	35.73 ± 0.80
35	24.01 ± 2.36	32.08 ± 0.69	30.02 ± 2.24	34.16 ± 2.05	16.04 ± 0.99	26.40 ± 0.82	9.51 ± 0.08	32.91 ± 0.79
36	10.30 ± 0.05	35.91 ± 1.05	14.31 ± 1.02	31.51 ± 1.55	7.65 ± 0.51	23.68 ± 0.71	11.65 ± 0.21	34.05 ± 0.54
37	8.30 ± 0.11	28.25 ± 0.88	15.39 ± 0.47	24.82 ± 1.87	11.47 ± 0.28	25.31 ± 0.92	12.07 ± 0.34	24.88 ± 0.91
38	6.85 ± 0.03	33.61 ± 0.63	12.00 ± 0.95	26.30 ± 1.03	9.01 ± 0.25	20.13 ± 0.74	10.04 ± 0.85	25.31 ± 0.18
39	7.05 ± 0.02	30.46 ± 1.52	14.30 ± 0.84	14.38 ± 0.97	10.81 ± 0.24	14.05 ± 0.31	8.33 ± 0.77	12.48 ± 0.07
40	9.71 ± 0.14	24.07 ± 0.51	11.61 ± 0.81	19.73 ± 0.92	7.16 ± 0.07	15.34 ± 0.25	7.05 ± 0.59	18.62 ± 0.10
41	6.69 ± 0.08	26.35 ± 0.69	12.05 ± 0.67	14.67 ± 1.05	6.07 ± 0.18	12.61 ± 0.09	4.00 ± 0.01	10.03 ± 0.07
42	2.51 ± 0.01	22.51 ± 0.31	16.38 ± 0.38	19.03 ± 1.17	4.30 ± 0.09	7.25 ± 0.07	3.17 ± 0.02	14.29 ± 0.08
43	4.36 ± 0.03	29.38 ± 0.24	14.06 ± 0.40	16.45 ± 0.95	5.03 ± 0.01	5.64 ± 0.04	4.03 ± 0.01	13.57 ± 0.05
44	3.22 ± 0.01	18.01 ± 0.22	8.55 ± 0.09	10.06 ± 0.72	3.19 ± 0.02	8.31 ± 0.09	3.43 ± 0.05	10.95 ± 0.06
45	4.85 ± 0.15	20.53 ± 0.18	11.37 ± 0.24	12.45 ± 0.74	4.13 ± 0.01	6.89 ± 0.06	4.09 ± 0.02	11.68 ± 0.05
46	5.01 ± 0.08	14.69 ± 0.12	4.15 ± 0.13	10.31 ± 0.55			3.03 ± 0.01	5.89 ± 0.03
47	4.65 ± 0.06	19.57 ± 0.14	3.85 ± 0.05	14.02 ± 0.62			3.14 ± 0.05	8.17 ± 0.02

Table 2 (continued)

Depth (cm)	Activity concentration (Bq kg^{-1})							
	Core-1		Core-2		Core-3		Core-4	
	^{137}Cs	^{210}Pb$_{ex}$	^{137}Cs	^{210}Pb$_{ex}$	^{137}Cs	^{210}Pb$_{ex}$	^{137}Cs	^{210}Pb$_{ex}$
48	3.08 ± 0.02	11.26 ± 0.07	3.62 ± 0.07	9.40 ± 0.24			4.91 ± 0.04	9.51 ± 0.05
49	4.23 ± 0.01	14.05 ± 0.21	4.08 ± 0.05	12.08 ± 0.27			3.12 ± 0.01	6.22 ± 0.03
50	2.55 ± 0.05	11.45 ± 0.13						
Median	29.61 ± 0.16	57.72 ± 3.61	32.65 ± 3.01	73.06 ± 2.20	28.77 ± 0.25.	62.05 ± 1.98	24.95 ± 2.06	71.22 ± 1.55
Minimum	2.51 ± 0.02	11.26 ± 0.07	3.62 ± 0.05	9.40 ± 0.24	3.19 ± 0.02	5.64 ± 0.04	3.03 ± 0.02	5.89 ± 0.03
Maximum	65.28 ± 4.38	218.42 ± 12.51	62.15 ± 5.31	230.42 ± 11.38	61.76 ± 4.28	191.28 ± 15.36	73.50 ± 5.27	305.22 ± 14.08

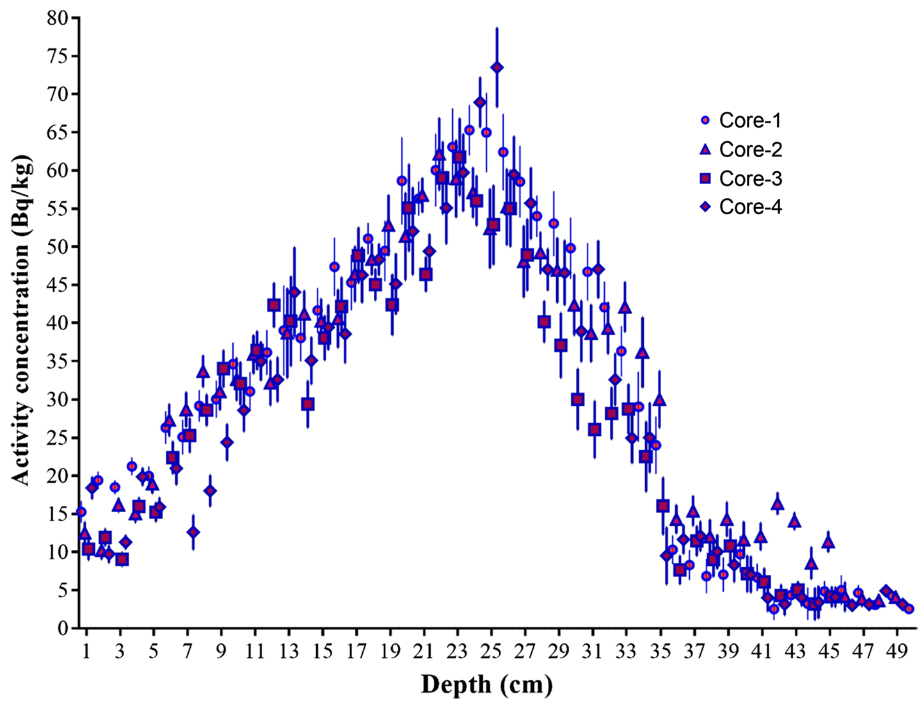

Fig. 3 Distribution of ^{137}Cs activity concentration in four core sediment profiles

in the Core-2 samples, from 5.64 ± 0.04 Bq kg^{-1} to 191.28 ± 15.36 Bq kg^{-1} and ^{226}Ra activity concentration was ranged from 1.53 ± 0.28 Bq kg^{-1} to 17.27 ± 1.28 Bq kg^{-1} in the Core-3 samples and from 5.89 ± 0.03 Bq kg^{-1} to 305.22 ± 14.08 Bq kg^{-1} and ^{226}Ra activity concentration was ranged from < MDA to 27.13 ± 1.55 Bq kg^{-1} in the Core-4 samples. ^{210}Pb$_{ex}$ activity concentration profiles from the four sampling locations are presented in Fig. 4.

Sedimentation rates estimation

According to our investigation, the first and second peaks of ^{137}Cs concentration in sediment profile ranged from 37 to 40 and 22 to 25 cm, respectively (Table 3). The first peak concern to significant fallout on a global scale began after the initial test in the early 1960s from nuclear weapons testing and then declined because of the performance of the international treaty banning like tests. The substantial second peak originated from Chernobyl accident fallout in 1986.

The analysis of ^{137}Cs activity concentration in sediment profile led us to the calculation of SR and SAR in the Anzali Lagoon. The calculation results are chronologically divided into two sections from 1963 to 1986 and after 1986. In the section from 1963 to 1986 interval, the range of SR and SAR were 0.52 ± 0.08 to 0.86 ± 0.15 cm year^{-1} with an average of 0.69 ± 0.07 cm year^{-1} and 0.08 ± 0.02 to 0.14 ± 0.07 g cm^{-2} year^{-1} with an average of 0.11 ± 0.05 g cm^{-2} year^{-1}, respectively. Whereas, the SR and SAR values range after 1986 were 0.78 ± 0.11 to 0.89 ± 0.15 cm year^{-1} (0.84 ± 0.13 cm year^{-1} on average) and 0.16 ± 0.01 to 0.18 ± 0.03 g cm^{-2} year^{-1} (0.17 ± 0.02 g cm^{-2} year^{-1} on average), respectively. (Table 3).

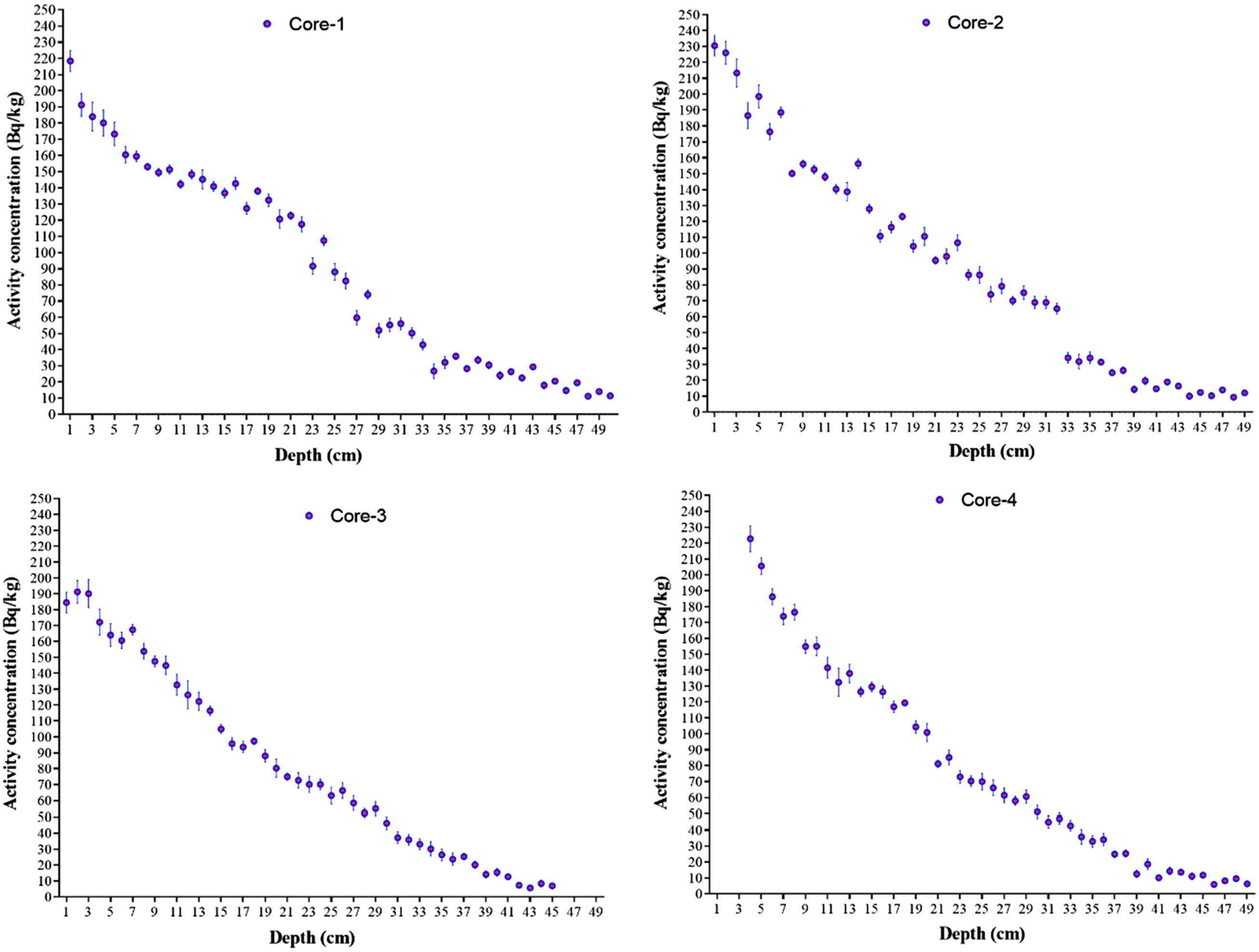

Fig. 4 Distribution of $^{210}Pb_{ex}$ activity concentration in four core sediment profiles

Table 3 The average sedimentation rates (SR) and average sediment accumulative rates (SARs) calculated using ^{137}Cs and $^{210}Pb_{ex}$ based in the Anzali Lagoon samples

Sample code	^{137}Cs 1st peak observed depth (cm)	^{137}Cs 2nd peak observed depth (cm)	^{137}Cs based average sedimentation rates (SR) (cm year^{-1})[a]		$^{210}Pb_{ex}$ based average sedimentation rates (SR) (cm year^{-1})[a]	^{137}Cs based Average sediment accumulative rates (SARs) (g cm^{-2} year^{-1})[a]		$^{210}Pb_{ex}$ based Average sediment accumulative rates (SARs) by CRS model (g cm^{-2} year^{-1})[a]
			1963–1986	After 1986		1963–1986	After 1986	
Core-1	40	24	0.69 ± 0.08	0.85 ± 0.12	0.75 ± 0.13	0.14 ± 0.07	0.17 ± 0.02	0.15 ± 0.02 (CRS)
Core-2	42	22	0.86 ± 0.15	0.78 ± 0.11	0.61 ± 0.18	0.08 ± 0.02	0.16 ± 0.01	0.12 ± 0.01 (CRS)
Core-3	39	23	0.68 ± 0.05	0.82 ± 0.12	1.03 ± 0.27	0.12 ± 0.01	0.16 ± 0.08	0.21 ± 0.03 (CRS)
Core-4	37	25	0.52 ± 0.08	0.89 ± 0.15	0.68 ± 0.05	0.10 ± 0.05	0.18 ± 0.03	0.14 ± 0.02 (CRS)
Average	–	–	0.69 ± 0.07	0.84 ± 0.13	0.76 ± 0.12	0.11 ± 0.05	0.17 ± 0.02	0.15 ± 0.02 (CRS)

[a]Uncertainties are considered within one standard deviation

The results of SR and SAR with $^{210}Pb_{ex}$ based inventories in sediment profile calculated and shown in Table 3. The value of SR was 0.61 ± 0.18 cm year^{-1} in core-2 and 1.03 ± 0.27 cm year^{-1} in core-3 with average 0.76 ± 0.12 cm year^{-1}. Also, the SAR value calculated by CRS were reported in Table 3. The CRS obtained values were ranged from 0.12 g cm^{-2} year^{-1} in core-2 to 0.21 g cm^{-2} year^{-1} in core-3.

Discussion

In this research, the sediments porosities taken from four sampling points have not any unusual event along to sediment profiles. Porosity varies between 0.72–0.81 from bottom to top levels in core-1, between 0.70–0.84 levels in core-2, between 0.75–0.85 levels in core-3 and between 0.71–0.88 levels in core-4. So, the sediments accumulated in the study area basement was homogenous. The relatively lower porosity at the bottom layers of cores might be due to sediment consolidation or compaction [6, 42, 43].

The result of ^{137}Cs and ^{226}Ra activity concentration in surface sediment (1–2 cm) were ranged between 9.74 to 19.34 Bq kg^{-1} and 3.85 to 34.11 Bq kg^{-1}, which is comparable with the last report from the Anzali wetland surface sediment 0.43- 63.35 Bq kg^{-1} and 18.06 to 33.36 Bq kg^{-1}, respectively. [44].

^{137}Cs activity concentration in all sediment profiles samples showed two peaks in layers. These peaks were observed in depth 40 cm and 24 cm, 42 cm, and 22 cm, 39 cm and 23 cm, and 37 cm and 25 cm for sample core-1, core-2, core-3, and core-4, respectively. Pulley and Foster et al. identified these peaks in Silsden sediment profiles at 28 cm and 13 cm depth [45]. Which these results were compared with other worldwide reports.

Ages calculated using $^{210}Pb_{ex}$ and ^{137}Cs technique are plotted against cumulative mass depth for each of the four cores (Fig. 5). In the core-1 profiles, among the CRS and CIC models, the CRS plot seems to have good agreement with ^{137}Cs technique-based chronology. The first peak of ^{137}Cs is 40 cm (1963), whereas according to the CRS model 40 cm is 1958. The second peak of ^{137}Cs indicated 24 cm (1986). Hence the CRS model provided 1982. The good agreement between the CRS model and ^{137}Cs technique-based chronology was reported by [46–51].

The ^{137}Cs technique with CRS and CIC models' plots has significant overlap in core-2, whereas in this core, ^{137}Cs was located in between the CRS model. The first peak of ^{137}Cs is 42 cm (1964), whereas according to CRS and CIC

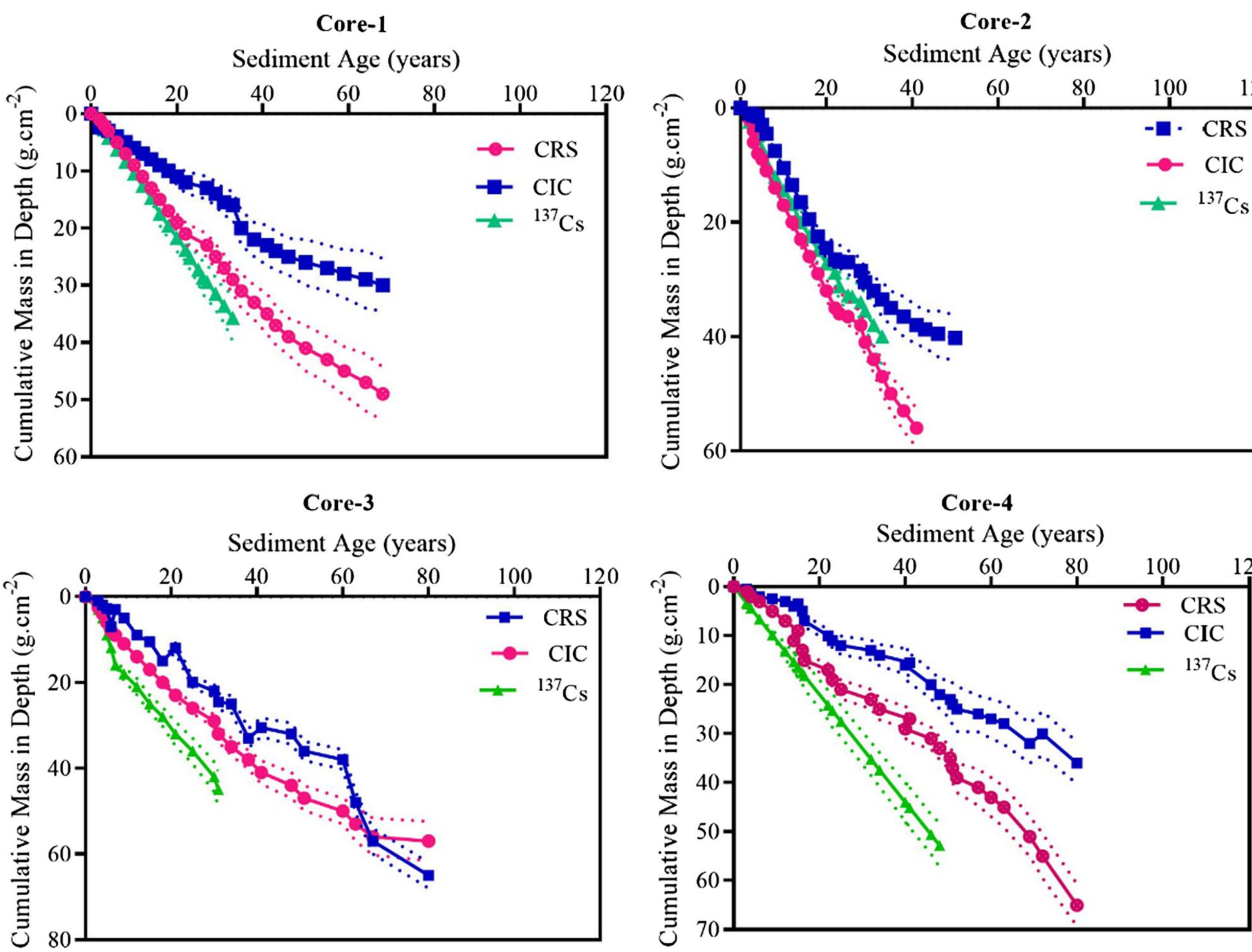

Fig. 5 Vertical profiles of sediment ages by cumulative mass in four cores obtained from CRS, CIC models and ^{137}Cs technique

models 42 cm fit in 1970 and 1954, respectively. The second peak of ^{137}Cs indicated 22 cm (1986), while the CRS model provided 1985 and CIC model fit in 1988. So, three methods have good agreements with together in core-2. The core-3 and core-4 results in CRS and CIC models are more distributed. There is no uniform consonant for the second peak of ^{137}Cs between cores. This inconsistency has been reported elsewhere [38, 52–55]. Only in cores 1 and 2 there is noticed a rapid trend alteration 45 and 55 years before, respectively.

The ^{137}Cs-peak based sediment accumulation rates (SAR) is generally based on one curve fitting method, based on the ^{137}Cs first peak corresponding to 1963 date. Also, the appearance of the ^{137}Cs radionuclide in sedimentary profiles returns to 1952 can be used as a time scale [56]. The 2nd peak of ^{137}Cs in sediment profiles is corresponding to Chernobyl accident fallout in 1986 [57, 58]. The average SR and SAR were calculated in two intervals. Whereas the average SR and SAR value in after 1986 interval was 22% and 54% more than 1963–1986, respectively. Where our value of 0.66 cm year^{-1} in 1963–1986 interval has good agreement with their report results. Also, the results of this study are within the range of SR value of 1.999 cm year^{-1} to 0.036 cm year^{-1} which reported in [59]. Eleftheriou et al. reported the SAR value between 0.21 and 0.6 cm year^{-1} (CRS model) and 0.13–0.42 cm year^{-1} (CIC model) in north-east Mediterranean [60]. As shown in Table 3, our average SR value in the Anzali Lagoon were higher than those measured in Greece (Lavrio) [61], Poland (Baltic Sea) [62]. Moreover, the results of this this study is lower than the last study in the Anzali Lagoon with the same characteristics with ^{137}Cs tracer technique [63].

Conclusions

This study has focused on recent concerns about unusual changes in the Anzali Lagoon ecosystem. For this purpose, the sediment porosities were computed and an exponentially decreasing trend observed in the porosity of upper sediment layers to deeper layers in all core sampling of the study area. Also, the distribution of ^{137}Cs and ^{210}Pb$_{ex}$ concentration in sediment profiles were measured in core samples. The ^{137}Cs technique and ^{210}Pb$_{ex}$ based models (CRS and CIC models) were applied to sediment chronology. The results of CRS, CIC models, and ^{137}Cs technique were compared. The CRS model has good compatible with the ^{137}Cs-peak-based technique in core-1 and core-2, whereas the CIC model only was agreed with results of ^{137}Cs-peak-based technique in core-2.

In this study, the SR and SAR of Anzali Lagoon were studied using natural ^{210}Pb$_{ex}$ based models and artificial ^{137}Cs-peak-based technique. Average obtained results of SR in the North area (core-4) of the lake was higher than the South area (core-2). This can be due to the gradient of the land surface of the Lagoon because the slope of the land is southern in this area. Also, the ^{137}Cs peak-based technique of SR values was calculated in two intervals of 1963–1986 and after 1986 years. The SR value of after 1986 was higher than 1963–1986 interval on average. Besides, this trend is also true with the results of SAR. Whereas the results showed that the average of SR and SAR values in after 1986 interval were 22% and 54% more than between 1963 and 1986, respectively. It could be due to floods and storms are occurring in the study area and human activities. Also, due to the lack of any available date in this area, the results of the present study will provide available and comparable data for the next studies.

Acknowledgements The authors would like to thank the Maritime Patrol of the study area that contributed to the sampling of sediment.

References

1. Colman SM, Baucom PC, Bratton JF, Cronin TM, McGeehin JP, Willard D, Zimmerman AR, Vogt PR (2002) Radiocarbon dating, chronologic framework, and changes in accumulation rates of Holocene estuarine sediments from Chesapeake Bay. Quat Res 57(1):58–70
2. Tylmann W, Bonk A, Goslar T, Wulf S, Grosjean M (2016) Calibrating 210Pb dating results with varve chronology and independent chronostratigraphic markers: problems and implications. Quat Geochronol 32:1–10
3. Corcoran M, Sherif MI, Smalley C, Li A, Rockne KJ, Giesy JP, Sturchio NC (2018) Accumulation rates, focusing factors, and chronologies from depth profiles of 210Pb and 137Cs in sediments of the Laurentian Great Lakes. J Great Lakes Res 44(4):693–704
4. Turner L, Delorme L (1996) Assessment of 210 Pb data from Canadian lakes using the CIC and CRS models. Environ Geol 28(2):78–87
5. Drexler JZ, Fuller CC, Archfield S (2018) The approaching obsolescence of 137Cs dating of wetland soils in North America. Quat Sci Rev 199:83–96
6. Kumar A, Rout S, Chopra MK, Mishra D, Singhal R, Ravi P, Tripathi R (2014) Modeling of 137Cs migration in cores of marine sediments of Mumbai Harbor Bay. J Radioanal Nucl Chem 301(2):615–626
7. Durham R, Joshi S (1980) The 210Pb and 137Cs profiles in sediment cores from Lakes Matagami and Quevillon, northwest Quebec, Canada. Can J Earth Sci 17(12):1746–1750
8. Snow MS, Snyder DC, Clark SB, Kelley M, Delmore JE (2015) 137Cs activities and 135Cs/137Cs isotopic ratios from soils at Idaho National Laboratory: a case study for contaminant source attribution in the vicinity of nuclear facilities. Environ Sci Technol 49(5):2741–2748. https://doi.org/10.1021/es5058852
9. Ritchie JC, McHenry JR (1990) Application of radioactive fallout cesium-137 for measuring soil erosion and sediment accumulation rates and patterns: a review. J Environ Qual 19(2):215–233
10. Matisoff G (2017) Activities and geochronology of (137)Cs in lake sediments resulting from sediment resuspension. J Environ Radioact 167:222–234. https://doi.org/10.1016/j.jenvrad.2016.11.015
11. Whicker JJ, Whicker FW, Jacobi S (1994) 137Cs in sediments of Utah lakes and reservoirs: effects of elevation, sedimentation rate and fallout history. J Environ Radioact 23(3):265–283

12. He Q, Walling D, Owens P (1996) Interpreting the 137Cs profiles observed in several small lakes and reservoirs in southern England. Chem Geol 129(1):115–132
13. Albrecht A, Reiser R, Lück A, Stoll J-MA, Giger W (1998) Radiocesium dating of sediments from lakes and reservoirs of different hydrological regimes. Environ Sci Technol 32(13):1882–1887
14. Saxén R, Ilus E (2008) Transfer and behaviour of 137Cs in two Finnish lakes and their catchments. Sci Total Environ 394(2–3):349–360
15. Ahn YS, Mizugaki S, Nakamura F, Nakamura Y (2006) Historical change in lake sedimentation in Lake Takkobu, Kushiro Mire, northern Japan over the last 300 years. Geomorphology 78(3–4):321–334
16. Mizugaki S, Nakamura F, Araya T (2006) Using dendrogeomorphology and 137Cs and 210Pb radiochronology to estimate recent changes in sedimentation rates in Kushiro Mire, Northern Japan, resulting from land use change and river channelization. CATENA 68(1):25–40
17. Mikelić IL, Oreščanin V, Škaro K (2017) Variation of sedimentation rate in the semi-enclosed bay determined by 137Cs distribution in sediment (Kaštela Bay, Croatia). J Environ Radioact 166:112–125
18. Schumm SA (1977) The fluvial system
19. Xu J (2003) Sedimentation rates in the lower Yellow River over the past 2300 years as influenced by human activities and climate change. Hydrol Process 17(16):3359–3371
20. Jafari N (2009) Ecological integrity of wetland, their functions and sustainable use. J Ecol Nat Environ 1(3):045–054
21. Rafiei B, Ghomi FA, Ardebili L, Sadeghifar M, Sharifi SHK (2012) Distribution of metals (Cu, Zn, Pb, and Cd) in sediments of the Anzali Lagoon, north Iran. Soil Sediment Contam Int J 21(6):768–787
22. Chen J, Pekker T, Wilson C, Tapley B, Kostianoy A, Cretaux JF, Safarov E (2017) Long-term Caspian Sea level change. Geophys Res Lett 44(13):6993–7001
23. Wang J, Du J, Baskaran M, Zhang J (2016) Mobile mud dynamics in the East China Sea elucidated using 210Pb, 137Cs, 7Be, and 234Th as tracers. J Geophys Res Oceans 121(1):224–239
24. Abbasi A, Mirekhtiary F (2013) Comparison of active and passive methods for radon exhalation from a high–exposure building material. Radiat Prot Dosim 157(4):570–574
25. Abbasi A (2013) Calculation of gamma radiation dose rate and radon concentration due to granites used as building materials in Iran. Radiat Prot Dosim 155(3):335–342
26. Başkaya H, Doğru M, Küçükönder A (2014) Determination of the 137Cs and 90Sr radioisotope activity concentrations found in digestive organs of sheep fed with different feeds. J Environ Radioact 134:61–65
27. Currie LA (1968) Limits for qualitative detection and quantitative determination. Application to radiochemistry. Anal Chem 40(3):586–593
28. Lépy M, Pearce A, Sima O (2015) Uncertainties in gamma-ray spectrometry. Metrologia 52(3):S123
29. Wright S, Howard B, Strand P, Nylén T, Sickel M (1999) Prediction of 137Cs deposition from atmospheric nuclear weapons tests within the Arctic. Environ Pollut 104(1):131–143
30. Smith J, Clarke R, Saxén R (2000) Time-dependent behaviour of radiocaesium: a new method to compare the mobility of weapons test and Chernobyl derived fallout. J Environ Radioact 49(1):65–83
31. Yan P, Shi P, Gao S, Chen L, Zhang X, Bai L (2002) 137Cs dating of lacustrine sediments and human impacts on Dalian Lake, Qinghai Province, China. CATENA 47(2):91–99
32. Almgren S, Isaksson M (2006) Vertical migration studies of 137Cs from nuclear weapons fallout and the Chernobyl accident. J Environ Radioact 91(1–2):90–102
33. Tsabaris C, Patiris D, Fillis-Tsirakis E, Kapsimalis V, Pilakouta M, Pappa F, Vlastou R (2015) Vertical distribution of 137Cs activity concentration in marine sediments at Amvrakikos Gulf, western of Greece. J Environ Radioact 144:1–8
34. Smith JT, Tagami K, Uchida S (2017) Time trends in radiocaesium in the Japanese diet following nuclear weapons testing and Chernobyl: implications for long term contamination post-Fukushima. Sci Total Environ 601:1466–1475
35. Sanchez-Cabeza J, Ruiz-Fernández A (2012) 210Pb sediment radiochronology: an integrated formulation and classification of dating models. Geochim Cosmochim Acta 82:183–200
36. Oldfield F, Appleby P (1984) A combined radiometric and mineral magnetic approach to recent geochronology in lakes affected by catchment disturbance and sediment redistribution. Chem Geol 44(1–3):67–83
37. Golosov VN, Walling DE, Konoplev AV, Ivanov MM, Sharifullin AG (2018) Application of bomb- and Chernobyl-derived radiocaesium for reconstructing changes in erosion rates and sediment fluxes from croplands in areas of European Russia with different levels of Chernobyl fallout. J Environ Radioact 186:78–89. https://doi.org/10.1016/j.jenvrad.2017.06.022
38. Kumar A, Hage-Hassan J, Baskaran M, Miller C, Selegean J, Creech C (2016) Multiple sediment cores from reservoirs are needed to reconstruct recent watershed changes from stable isotopes (δ13C and δ15 N) and C/N ratios: case studies from the mid-western United States. J Paleolimnol 56(1):15–31
39. Kumar A, Hage-Hassan J, Baskaran M, Miller C, Selegean J, Creech C (2016) Multiple sediment cores from reservoirs are needed to reconstruct recent watershed changes from stable isotopes (δ13C and δ15 N) and C/N ratios: case studies from the mid-western United States. J Paleolimnol 56(1):15–31
40. Appleby P, Oldfield F, Thompson R, Huttunen P, Tolonen K (1979) 210Pb dating of annually laminated lake sediments from Finland. Nature 280(5717):53
41. Robbins JA, Edgington DN (1975) Determination of recent sedimentation rates in Lake Michigan using Pb-210 and Cs-137. Geochim Cosmochim Acta 39(3):285–304
42. Kumar A, Rout S, Karpe R, Mishra MK, Narayanan U, Singhal RK, Ravi PM, Tripathi RM (2015) Inventory, fluxes and residence times from the depth profiles of naturally occurring 210 Pb in marine sediments of Mumbai Harbor Bay. Environ Earth Sci 73(8):4019–4031
43. Kumar A, Rout S, Singhal R, Ravi P, Tripathi R (2016) Sediment accumulation and bio-diffusion mixing rates derived from excess 210Pb and 137Cs profiles in sediment cores of Mumbai Harbor Bay. J Coast Conserv 20(4):289–297
44. Zare MR, Kamali M, Fallahi Kapourchali M, Bagheri H, Khoram Bagheri M, Abedini A, Pakzad HR (2016) Investigation of (235)U, (226)Ra, (232)Th, (40)K, (137)Cs, and heavy metal concentrations in Anzali international wetland using high-resolution gamma-ray spectrometry and atomic absorption spectroscopy. Environ Sci Pollut Res Int 23(4):3285–3299. https://doi.org/10.1007/s11356-015-5473-8
45. Pulley S, Foster IDL, Collins AL, Zhang Y, Evans J (2018) An analysis of potential controls on long-term 137Cs accumulation in the sediments of UK lakes. J Paleolimnol 60(1):1–30. https://doi.org/10.1007/s10933-017-0016-6
46. Ahn YS (2018) Recent changes in sedimentation rate in three lakes of Ishikari Wetland, Northern Japan determined by 210Pb dating. Water Resour 45(5):795–802
47. Li Z, Xu X, Zhang Y, Wang K, Zeng P (2019) Reconstructing recent changes in sediment yields from a typical karst watershed in southwest China. Agric Ecosyst Environ 269:62–70
48. Mejjad N, Laissaoui A, El-Hammoumi O, Fekri A, Amsil H, El-Yahyaoui A, Benkdad A (2018) Geochemical, radiometric, and environmental approaches for the assessment of the intensity

and chronology of metal contamination in the sediment cores from Oualidia lagoon (Morocco). Environ Sci and Pollut Res 25(23):22872–22888
49. Haliuc A, Feurdean A, Mîndrescu M, Frantiuc A, Hutchinson SM (2018) Impacts of forest loss in the eastern Carpathian Mountains: linking remote sensing and sediment changes in a mid-altitude catchment (Red Lake, Romania). Reg Environ Change 19(2):461–475
50. Bao K, Wang G, Pratte S, Mackenzie L, Klamt A-M (2018) Historical variation in the distribution of trace and major elements in a Poor Fen of Fenghuang Mountain, NE China. Geochem Int 56(10):1003–1015
51. Moir KE, Hickey MBC, Leavitt PR, Ridal JJ, Cumming BF (2018) Paleolimnological proxies reveal continued eutrophication issues in the St. Lawrence River area of concern. J Great Lakes Res 44(3):357–366
52. Jweda J, Baskaran M (2011) Interconnected riverine–lacustrine systems as sedimentary repositories: Case study in southeast Michigan using 210Pb and 137Cs-based sediment accumulation and mixing models. J Great Lakes Res 37(3):432–446
53. Lan B, Zhang D, Yang Y (2018) Lacustrine sediment chronology defined by 137Cs, 210Pb and 14C and the hydrological evolution of Lake Ailike during 1901–2013, northern Xinjiang, China. CATENA 161:104–112
54. Sayer CD, Davidson TA, Rawcliffe R, Langdon PG, Leavitt PR, Cockerton G, Rose NL, Croft T (2016) Consequences of fish kills for long-term trophic structure in shallow lakes: implications for theory and restoration. Ecosystems 19(7):1289–1309
55. Marzecová A, Avi E, Mikomägi A, Koff T (2017) Ecological response of a shallow boreal lake to biomanipulation and catchment land-use: integrating paleolimnological evidence with information from limnological surveys and maps. J Paleolimnol 57(1):1–18
56. Baskaran M, Miller CJ, Kumar A, Andersen E, Hui J, Selegean JP, Creech CT, Barkach J (2015) Sediment accumulation rates and sediment dynamics using five different methods in a well-constrained impoundment: case study from Union Lake, Michigan. J Great Lakes Res 41(2):607–617. https://doi.org/10.1016/j.jglr.2015.03.013
57. Reyss J-L, Mangeret A, Courbet C, Bassot S, Alcalde G, Thouvenot A, Guillevic J (2016) Estimation of sedimentation rates based on the excess of radium 228 in granitic reservoir sediments. J Environ Radioact 162:8–13
58. Golosov V, Ivanova N, Gusarov A, Sharifullin A (2017) Assessment of the trend of degradation of arable soils on the basis of data on the rate of stratozem development obtained with the use of 137Cs as a chronomarker. Eurasian Soil Sci 50(10):1195–1208
59. Sert I, Ozel FE, Yaprak G, Eftelioglu M (2015) Determination of the latest sediment accumulation rates and pattern by performing 210Pb models and 137Cs technique in the Lake Bafa, Mugla, Turkey. J Radioanal Nucl Chem 307(1):313–323. https://doi.org/10.1007/s10967-015-4234-y
60. Eleftheriou G, Tsabaris C, Papageorgiou DK, Patiris DL, Androulakaki EG, Pappa FK (2018) Radiometric dating of sediment cores from aquatic environments of north-east Mediterranean. J Radioanal Nucl Chem 316(2):655–671
61. Pappa FK, Tsabaris C, Patiris DL, Androulakaki EG, Betsou GC, Michalopoulou V, Kokkoris M, Vlastou R (2018) Historical trends and assessment of radionuclides and heavy metals in sediments near an abandoned mine, Lavrio, Greece. Environ Sci Pollut Res 25(30):30084–30100
62. Zaborska A, Winogradow A, Pempkowiak J (2014) Caesium-137 distribution, inventories and accumulation history in the Baltic Sea sediments. J Environ Radioact 127:11–25
63. Vavdare KS, Sedghi H, Sarraf A (2019) Determination of Sedimentation Rate in Anzali Lagoon of Northern Iran Using Cs-137 Tracer Technique. Appl Ecol Environ Res 17(1):1337–1347